THE JOURNAL OF PHYSICAL CHEMISTRY LETTERS
A JOURNAL OF THE AMERICAN CHEMICAL SOCIETY

pubs.acs.org/JPCL

Letter

In_2Se_3, In_2Te_3, and $In_2(Se,Te)_3$ Alloys as Photovoltaic Materials

Wei Li,* Xue-Fen Cai, Nicholas Valdes, Tianshi Wang, William Shafarman, Su-Huai Wei, and Anderson Janotti*

Cite This: *J. Phys. Chem. Lett.* 2022, 13, 12026−12031

Read Online

ACCESS | Metrics & More | Article Recommendations

ABSTRACT: In its lowest-energy three-dimensional (3D) hexagonal crystal structure (γ phase), In_2Se_3 has a direct band gap of ∼1.8 eV and displays high absorption coefficient, making it a promising semiconductor material for optoelectronics. Incorporation of Te allows for tuning the band gap, adding flexibility to device design and extending the application range. Here we report results of hybrid density functional theory calculations to assess the electronic and optical properties of γ-In_2Se_3, γ-In_2Te_3, and γ-$In_2(Se_{1-x}Te_x)_3$ alloys, and initial experiments on the growth and characterization of γ-In_2Se_3 thin films. The predicted band gap of 1.84 eV for γ-In_2Se_3 is in good agreement with the absorption onset derived from transmission and reflection spectra of thin films. We show that incorporation of Te gives γ-$In_2(Se_{1-x}Te_x)_3$ alloys with a band gap ranging from 1.84 eV down to 1.23 eV, thus covering the optimal band gap range for single-junction solar cells. In addition, the γ-In_2Se_3/γ-$In_2(Se_{1-x}Te_x)_3$ bilayer could be employed in tandem solar-cell architectures absorbing at $E_g \approx 1.8$ eV and at $E_g \leq 1.4$ eV, toward overcoming the ∼33% efficiency set by the Shockley-Queisser limit for single junction solar cells. We also discuss band gap bowing and mixing enthalpies, aiming at adding γ-In_2Se_3, γ-In_2Te_3, and γ-$In_2(Se_{1-x}Te_x)_3$ alloys to the available toolbox of materials for solar cells and other optoelectronic applications.

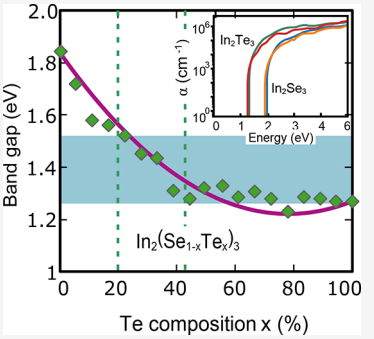

In the search for novel semiconductor materials for photovoltaic (PV) applications, it is desirable to focus on compounds with a simple formula unit (i.e., containing few elements) and relatively simple crystal structure to minimize the number of possible point defects, such as vacancies, interstitials, and antisites, that can act as recombination centers. For instance, Si and CdTe are the two materials that dominate the PV market, whereas the multinaries ternaries CIGS and CZTS have struggled in terms of efficiency in devices,[1−5] in part due to their complicated composition and crystal structure. Inspired by the virtues and current limitations of CdTe,[6] regarding the ease of manufacture but difficulties controlling doping levels, here we focus on In_2Se_3 and In_2Te_3 as candidates for PV materials. In_2Se_3 crystallizes in a 3D defect wurtzite-like structure (γ-In_2Se_3, Figure 1) at room temperature.[7−9] It has a direct band gap of ∼1.8 eV and displays a high absorption coefficient in the visible-light range.[7,9−15] In_2Se_3 thin film has been used as a precursor layer in coevaporation of $CuInSe_2$-based solar cells,[16] as well as a buffer layer to replace CdS in Mo/CIS/In_2Se_3/ZnO device structures, showing higher open-circuit voltage than the Mo/CIS/CdS/ZnO structure.[17] The band gap of In_2Se_3 can be lowered by adding Te[18] in the form of $In_2(Se,Te)_3$ alloys, covering the spectrum region suitable for solar cell applications. Besides this limited information, details of the electronic and optical properties of In_2Se_3, In_2Te_3, and $In_2(Se,Te)_3$ alloys have remained largely unexplored.

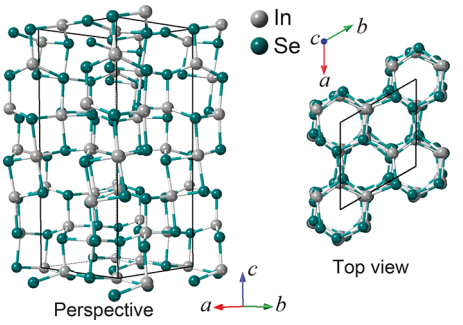

Figure 1. Crystal structure of γ-In_2Se_3, showing a perspective and a top view of the 3D defective wurtzite crystal structure with space group $P6_1$.

Here we report a combination of experimental and computational studies on γ-In_2Se_3 and γ-$In_2(Se_{1-x}Te_x)_3$ alloys, focusing on their structural, electronic, and optical properties, with the aim of developing these materials for electronic and optoelectronic applications. First, we discuss the growth and

Received: September 28, 2022
Accepted: December 15, 2022
Published: December 21, 2022

basic characterization of In_2Se_3 thin films, followed by a discussion of hybrid density functional calculations of structure and electronic properties of γ-In_2Se_3 and a comparison with experimental data. We then discuss the calculated absorption coefficients and band alignment between γ-In_2Se_3, γ-In_2Te_3, and other more conventional chalcogenide semiconductors, such as CdTe and $CuInSe_2$. Finally, we discuss the stability and electronic properties of γ-$In_2(Se_{1-x}Te_x)_3$ alloys, showing that the band gap can be adjusted from 1.84 eV down to 1.23 by changing the Te concentration, passing through the optimum range of direct band gaps for a single-junction solar cell. We then conclude with a discussion on how this material system offers new opportunities for innovative architectures and device design.

Thin film of γ-In_2Se_3 was grown on soda lime glass substrates by thermal coevaporation of In and Se. The growth lasted 30 min; the substrate temperature was set to 350 °C to form films with a thickness of 1 μm. Composition was verified by X-ray fluorescence. Spectrophotometry was performed to measure transmission and reflection in the wavelength range of 300−2000 nm, and the absorption coefficient was determined from the reflection and transmission spectra.[19]

The calculations were based on the density functional theory[20,21] as implemented in the VASP code.[22,23] The interactions between the valence electrons and the ionic cores are described using projector augmented wave (PAW) potentials.[24,25] We used a kinetic energy cutoff of 320 eV for the plane wave basis set. Structure optimization was performed using the Perdew−Burke−Ernzerhof functional revised for solids (PBEsol)[26] on a Γ-centered 6 × 6 × 2 mesh for the 30-atom primitive cells of γ-In_2Se_3 and γ-In_2Te_3, and equivalent k-point mesh for supercells for the γ-$In_2(Se_{1-x}Te_x)_3$ alloys. Once the ionic positions were determined using the PBEsol functional, we calculated the electronic structure and dielectric functions using the HSE06 functional,[27,28] including the effects of spin−orbit coupling. Note that the band gaps consistently calculated in HSE06 using optimized lattice parameters also in HSE06 are only slightly higher in energy by less than 0.15 eV. Contributions from excitons and phonon-assisted optical transitions to the absorption coefficients were not included in the present work; exciton binding energies are expected to be less than 100 meV,[29] and phonon-assisted optical transitions would significantly modify the spectrum near the band edges if the indirect band gap were much lower than the direct band gap, which is not the case as discussed later in the text. Therefore, inclusion of these effects will not change our main conclusions. To obtain a good description of optical band gap threshold, we use the tetrahedron method with a small complex shift of 1 meV in the Kramers−Kronig transformation.[30]

For simulating the $In_2(Se_{1-x}Te_x)_3$ random alloys we employed special quasi-random structures (SQS)[31,32] obtained using the Alloy Theoretic Automated Toolkit (ATAT).[33] This approach is based on a Monte Carlo simulated annealing loop with an objective function that seeks to perfectly match the maximum number of atomic correlation functions of the random alloys.[33] Here we use supercells with 90 atoms for representing $In_2(Se_{1-x}Te_x)_3$ alloys.

The defective wurtzite crystal structure of γ-In_2Se_3 (and γ-In_2Te_3) with space group $P6_1$ is shown in Figure 1. This crystal structure is built up of $In(1)Se_5$ trigonal bipyramids and $In(2)Se_4$ tetrahedra,[34] which are connected by common corners and edges resulting in a distorted wurtzite-like structure, i.e., a wurtzite structure missing one-third of cation sites. The vacant sites are orderly arranged forming a screw along the c axis (vacancy ordered in screw form, or VOSF phase).[7,35,36] The calculated equilibrium lattice parameters for γ-In_2Se_3 are a = 7.179 Å and c = 19.412 Å, in good agreement with experimental values a = 7.129 Å and c = 19.381 Å.[34] For γ-In_2Te_3, the calculated lattice parameters are a = 7.632 Å and c = 20.980 Å. Experimental data are not available in this case.

The calculated electronic structure for γ-In_2Se_3 and γ-In_2Te_3 are shown in Figure 2a,b. In the case of γ-In_2Se_3, we find a

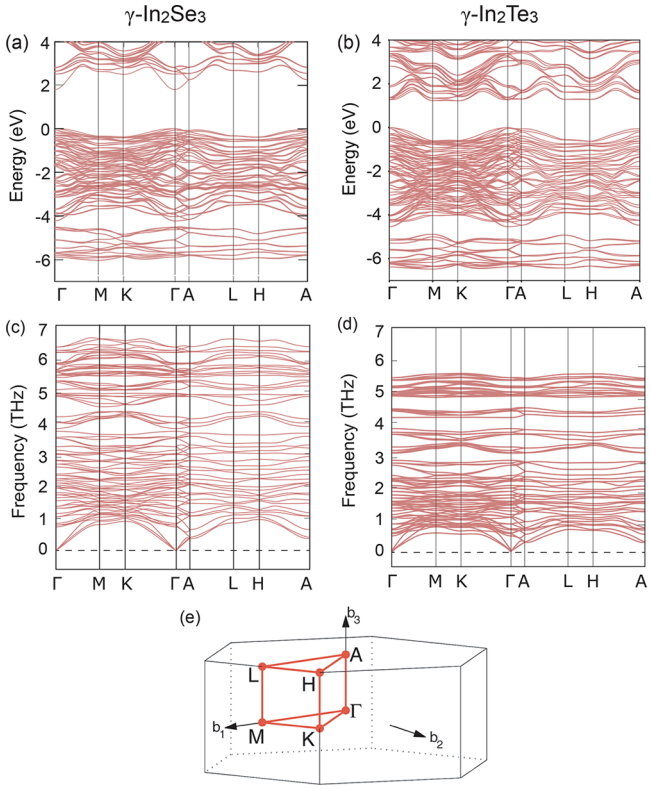

Figure 2. Electronic band structure and phonon dispersion of γ-In_2Se_3 and γ-In_2Te_3. Calculated electronic structure of (a) γ-In_2Se_3 showing a direct band gap at Γ and (b) of γ-In_2Te_3 showing the direct band gap at Γ very close in energy to the indirect band gap Γ-K. Calculated phonon dispersion of (c) γ-In_2Se_3 and (d) γ-In_2Te_3 along high-symmetry directions; the absence of negative phonon frequencies indicates the structural stability of the two compounds in the 3D γ phase. (e) Brillouin zone showing the path and high-symmetry k points.

direct band gap of 1.84 eV at the Γ point, in good agreement with the onset of optical absorption shown in Figure 3a and previously reported values of 1.8−1.9 eV.[11−13] Consistently using the optimized HSE06 lattice parameters we obtain a gap of 1.88 eV, which is only slightly larger. Previous DFT-GGA calculations for γ-In_2Se_3 showed a band gap of ∼1.0 eV.[37] However, GGA functionals are known to underestimate band gaps. We find that the lowest conduction band originates from In 5s orbitals, while the highest valence band originates mainly from Se 4p orbitals. The calculated effective electron masses are 0.136 m_e and 0.148 m_e, respectively, along the in-plane and out-of-plane directions, based on a parabolic fit to the band structure around the CBM. In the case of γ-In_2Te_3, we find an indirect band gap of 1.23 eV, with the conduction-band minimum (CBM) at K, and a direct gap of 1.27 eV at Γ is only

https://doi.org/10.1021/acs.jpclett.2c02975
J. Phys. Chem. Lett. 2022, 13, 12026−12031

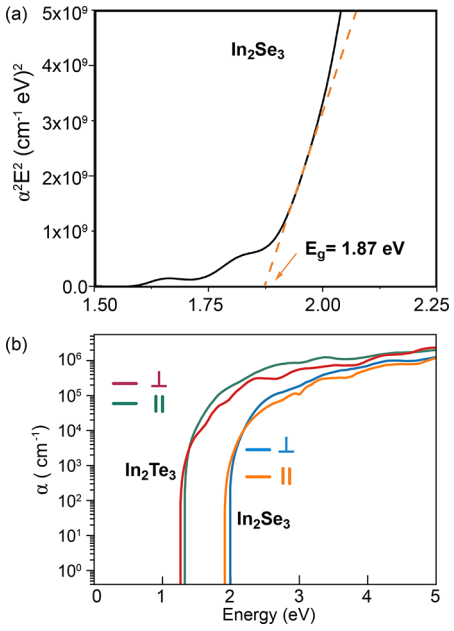

Figure 3. Optical properties of γ-In_2Se_3 and γ-In_2Te_3: (a) Tauc plot of the optical absorption derived from the transmission and reflection spectra of the In_2Se_3 thin film, indicating a gap of 1.87 eV. (b) Calculated absorption coefficient (α) of bulk γ-In_2Se_3 and γ-In_2Te_3 in log scale, for light polarization perpendicular ($\perp$) and parallel $\parallel$ to the c_{hex} axis.

slightly lower than at the Γ point by 0.04 eV. Note that our HSE06 calculations using the HSE06 optimized lattice parameters give a direct band gap at Γ of 1.34 eV, with the indirect gap Γ-K slightly higher in energy. Using the HSE06 lattice parameters, the indirect gap Γ-K is 1.38 eV, and the direct gap at Γ is 1.34 eV, inverting the order. Similar to In_2Se_3, the lowest energy conduction band is derived from In 5s orbitals, and the valence-band maximum (VBM) at Γ is mainly derived from Te 5p orbitals.

We verified the structural stability of the γ phase of In_2Se_3 and In_2Te_3 by inspecting their phonon spectra. The phonon dispersion calculations were obtained using a combination of VASP and phonopy.[38] In these calculations, the dynamic matrices and second order interatomic force constants (IFCs) are computed on a 8 × 8 × 8 q-point mesh. We generate 210 displaced supercells, each with 240 atoms, with the atomic displacements of 0.02 Å. The calculated phonon dispersions of γ-In_2Se_3 and γ-In_2Te_3, shown in Figure 2c,d, reveal no trace of imaginary frequency, indicating that our optimized structure for γ-In_2Se_3 represents a minimum-energy structure, consistent with experimental results, indicating that this phase is structurally stable.[7−9]

For the optical properties, we show the absorption spectra of γ-In_2Se_3 and γ-In_2Te_3 in Figure 3. A Tauc plot of the optical absorption of the In_2Se_3 thin film, obtained from measured transmission and reflection spectra, is shown in Figure 3a, with a direct band gap of 1.87 eV. For comparison, the calculated absorption coefficients α of bulk γ-In_2Se_3 and γ-In_2Te_3 are shown in Figure 3b. We find a good agreement between the calculated band gap of 1.84 eV and the value of 1.87 eV extracted from the Tauc plot.[39−41]

Due to the hexagonal crystal structure, the absorption coefficient is anisotropic, but it shows small differences for light polarization parallel vs perpendicular to the c_{hex} axis. The absorption coefficients of γ-In_2Se_3 and γ-In_2Te_3, derived from the real and imaginary parts of the dielectric function, rapidly increase for photon energies above the band gap and are comparable to those of conventional III−V and II−VI semiconductors. For γ-In_2Te_3, we note that the calculated onset at 1.27 eV in the absorption coefficient occurs at photon energies that are only slightly higher than the calculated fundamental indirect band gap.

For semiconductors, besides the band gap, it is essential to know the position of the valence and conduction-band edges in an absolute energy scale, and the band alignment to other common semiconductors for designing contacts and heterojunctions. Thus, we calculated the position of the band edges of γ-In_2Se_3 and γ-In_2Te_3 with respect to the vacuum level using the following procedure: first we built slabs for β-In_2Se_3 and β-In_2Te_3 constraining the volume per formula unit to be the same as that of γ-In_2Se_3 and γ-In_2Te_3, respectively. The β crystal structure is the same as that of Bi_2Se_3, which is a hexagonal two-dimensional layered structure formed of quintuple layers,[44] with a natural cleavage plane perpendicular to the c-axis. Since the volume per formula unit of the constructed β phase is constrained to be the same of that of the γ phase, they have the same average electrostatic potential. From the slab of this constrained β phase, we obtain the average electrostatic potential in a bulk region with respect to the vacuum level. We then combine the top of the VBM of the γ phase with respect to the average electrostatic potential in a bulk calculation, and the position of the average electrostatic potential of the β phase with respect to a vacuum to obtain the position of the VBM of the γ phase with respect to a vacuum. The results for γ-In_2Se_3 and γ-In_2Te_3 are shown in Figure 4,

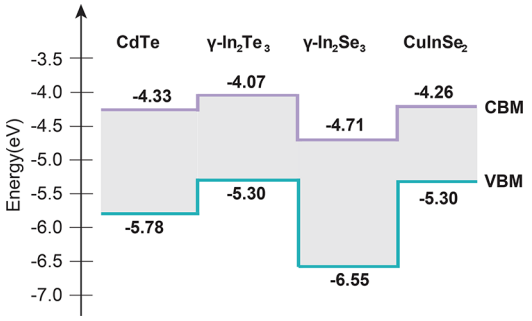

Figure 4. Band alignments and band edge positions with respect to a vacuum for γ-In_2Se_3 and γ-In_2Te_3, compared to $CuInSe_2$ (from ref 42) and CdTe (from ref 43), which are two important absorber materials in thin-film solar cells.

along with the values for CdTe and $CuInSe_2$ from the literature.[42,43] From the results, we note that the valence-band maximum of γ-In_2Te_3 is 1.25 higher than that of γ-In_2Se_3, which is attributed to the higher energy of Te 5p than the Se 4p orbital. This difference is larger than those between CdTe and CdSe and between ZnTe and ZnSe.[43,45] This is attributed to the stronger p-d coupling in the II−VI compounds that pushes up the VBM,[45,46] and it is stronger in the selenides than in the tellurides, reducing the valence band offset between them. The p-d interaction is weaker in γ-In_2Se_3 and γ-In_2Te_3 due to the stoichiometry (50% more anions than cations) and lower symmetry of the defective wurtzite crystal structure.

As shown in Figure 4, we find that the VBM of γ-In_2Te_3 is higher than that of CdTe; this is due to Te being 3-fold coordinated in γ-In_2Te_3, resulting in a nonbonding or lone-pair

https://doi.org/10.1021/acs.jpclett.2c02975
J. Phys. Chem. Lett. 2022, 13, 12026−12031

character of the VBM that is higher in energy than that of CdTe with a mainly Te *p*-Cd p bonding character. Note that CdTe is a material that is used in thin film solar cells, and one of the current limitations of CdTe-based solar cells is the efficiency of p-type doping. Having a VBM ∼ 0.5 eV higher than that of CdTe, we expect that it would be easier to dope γ-In_2Te_3 p-type, thus making this material itself a promising material for thin film solar cells, despite having a smaller band gap than CdTe.

Having established the structural, electronic, and optical properties of bulk γ-In_2Se_3 and γ-In_2Te_3, we now discuss the basic properties of γ-$In_2(Se_{1-x}Te_x)_3$ alloys. We simulate these random alloys using SQS structures in a supercell of 90 atoms, varying the Se/Te concentrations in steps of $\Delta x = 0.056$ (3/54), from $x = 0$ (γ-In_2Se_3) to $x = 1$ (γ-In_2Te_3). One example of such SQS structure for $x = 0.33$ (18/54) is shown in Figure 5a.

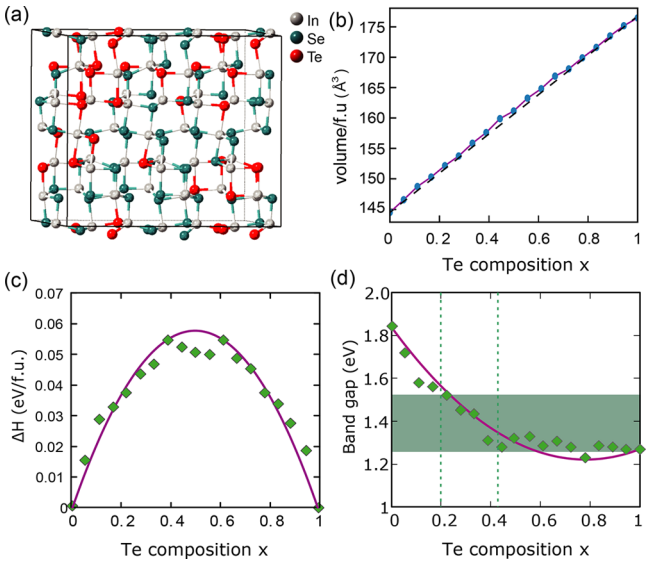

Figure 5. Structure, volume, mixing enthalpy, and band gap of γ-$In_2(Se_{1-x}Te_x)_3$ alloys. The structure in (a) represents a SQS structure for $x = 0.33$; the volume per formula unit of the alloys in (b) follows Vegard's law; the mixing enthalpy per formula unit as a function of Te concentration x in (c) is relatively low and comparable to other semiconductor alloy systems for which mixing over the whole concentration range has been observed. (d) Band gap of γ-$In_2(Se_{1-x}Te_x)_3$ alloys as a function of Te concentration x.

In Figure 5b we show the variation of the volume per formula unit of γ-$In_2(Se_{1-x}Te_x)_3$ alloys as a function of Te concentration x, indicating that these alloys closely follow Vegard's law.[47]

The ease of forming γ-$In_2(Se_{1-x}Te_x)_3$ alloys is, in part, determined by the mixing enthalpy, defined by

$$\Delta H_f[x] = E[x] - xE[In_2Se_3] - (1-x)E(In_2Te_3) \quad (1)$$

where $E[x]$ is the total energy of the γ-$In_2(Se_{1-x}Te_x)_3$ SQS supercell for a given x, $E(In_2Se_3)$ is the total energy of bulk γ-In_2Se_3 and $E(-In_2Te_3)$ is the total energy of bulk γ-In_2Te_3 using the same supercell size and k-mesh of the SQS structure. The results are shown in Figure 5c. We find that the mixing enthalpies are all positive and comparable to those of III−V-based alloys,[48] where uniform mixing have been observed for all alloy concentrations. The positive sign of ΔH_f indicates that the ground state of these alloys at $T = 0$ corresponds to phase separation into the binary constituents. However, since the formation enthalpies are relatively low, these alloys are likely to be stabilized through entropy at finite temperatures for the entire range of Te compositions.

The calculated band gap of γ-$In_2(Se_{1-x}Te_x)_3$ alloys as a function of composition x is shown in Figure 5d. We note that these results also include the effects of spin−orbit coupling. Here we only discuss the direct band gap at Γ in the alloys, despite the conduction-band minimum at K and at Γ being very close in energy in γ-In_2Te_3. The calculated bowing parameter b, defined as,[49]

$$E_g[x] = (1-x)E_g(In_2Se_3) + xE_g(In_2Te_3) - bx(1-x) \quad (2)$$

is 1.0 eV, which is close to other chalcogenide alloys such as (Cd,Se)Te (0.83 eV) and (Zn,Se)Te (1.23 eV).[46,50,51]

The band gap of γ-$In_2(Se_{1-x}Te_x)_3$ rapidly decreases with Te composition for small x, reaching around 1.3 eV for $x = 0.4$. For higher Te concentrations, i.e., $x > 0.4$, the gap remains within 0.1 eV of the gap of γ-In_2Te_3 and has a minimum band gap of 1.2 eV at $x = 0.8$. We attribute this behavior to the large difference between the energy of the Se/Te valence p orbitals, i.e., adding small amounts of Te to γ-In_2Se_3 leads to an isovalent Te-related band that is expected to be much higher in energy than the host valence band. Such a high VBM of the alloy not only reduces the band gap, but also facilitates p-type doping as in pure γ-In_2Te_3. Conversely, adding small amounts of Se to γ-In_2Te_3 would lead to an isovalent Se-related band below the VBM of the host, causing only small changes in the band gap.

Finally, we note that the band gap of γ-$In_2(Se_{1-x}Te_x)_3$ alloys can be tailored to be in the range of 1.2−1.5 eV for Te concentration between 20% and 100%, which is accepted as the optimum range of band gaps for single junction solar cells. One could also combine γ-In_2Se_3 or low Te content γ-$In_2(Se_{1-x}Te_x)_3$ alloys with high Te content alloys in tandem architectures, so the efficiency could surpass the ∼33% Shockley-Queisser limit for single-junction devices. Doping p type could be achieved using column-II acceptors, such as Mg, Ca, Zn, Cd, etc., yet such studies combined with native point defects are left for future work.

In summary, we investigated the structural, electronic, and optical properties of γ-In_2Se_3, and predicted the properties of γ-In_2Te_3, and γ-$In_2(Se_{1-x}Te_x)_3$ alloys, aiming at developing these materials for photovoltaic and other optoelectronic applications. γ-In_2Se_3 has a direct band gap of 1.84 eV, in good agreement with the onset in the absorption spectrum, whereas γ-In_2Te_3 has an indirect band gap of 1.23 eV, with the direct band gap at Γ being only 0.04 eV higher. The absorption coefficients of γ-In_2Se_3 and γ-In_2Te_3 are very high in the visible light range, reaching 10^5 cm^{-1} at ∼1 eV above the band gap energy. The valence band of γ-In_2Te_3 is predicted to be higher than that of CdTe, indicating that this material can be easily doped p-type. γ-$In_2(Se_{1-x}Te_x)_3$ alloys are predicted to easily form, with a maximum mixing enthalpy of 52 meV/f.u., similar to other semiconductor alloys for which mixing over the whole concentration range has been observed. The band gap of γ-$In_2(Se_{1-x}Te_x)_3$ alloys rapidly decreases with increasing Te composition, falling in the range of 1.2−1.5 eV for Te concentrations higher than ∼20%, which is optimal for single junction solar cells.[52] With such a high Te concentration, the VBM is also high enough to facilitate p-type doping. Our work thus indicates that the γ-$In_2(Se_{1-x}Te_x)_3$ alloy system is promising for photovoltaic applications.

https://doi.org/10.1021/acs.jpclett.2c02975
J. Phys. Chem. Lett. 2022, 13, 12026−12031

AUTHOR INFORMATION

Corresponding Authors

Wei Li − *Department of Materials Science & Engineering, University of Delaware, Newark, Delaware 19716, United States; Computer, Computational, and Statistical Sciences Division, Los Alamos National Laboratory, Los Alamos, New Mexico 87545, United States*; Email: wei_li@lanl.gov

Anderson Janotti − *Department of Materials Science & Engineering, University of Delaware, Newark, Delaware 19716, United States*; orcid.org/0000-0002-0358-2101; Email: janotti@udel.edu

Authors

Xue-Fen Cai − *Department of Materials Science & Engineering, University of Delaware, Newark, Delaware 19716, United States*

Nicholas Valdes − *Department of Materials Science & Engineering and Institute of Energy Conversion, University of Delaware, Newark, Delaware 19716, United States*; orcid.org/0000-0002-4116-5317

Tianshi Wang − *Department of Materials Science & Engineering and Institute of Energy Conversion, University of Delaware, Newark, Delaware 19716, United States*

William Shafarman − *Department of Materials Science & Engineering and Institute of Energy Conversion, University of Delaware, Newark, Delaware 19716, United States*; orcid.org/0000-0002-8937-4775

Su-Huai Wei − *Beijing Computational Science Research Center, Beijing 100193, China*; orcid.org/0000-0003-1563-4738

Complete contact information is available at: https://pubs.acs.org/10.1021/acs.jpclett.2c02975

Notes

The authors declare no competing financial interest.

ACKNOWLEDGMENTS

This work was supported by the National Science Foundation Faculty Early Career Development Program DMR-1652994. This research was also supported by the eXtreme Science and Engineering Discovery Environment (XSEDE) facility, National Science Foundation grant number ACI-1053575 and the Information Technologies (IT) resources at the University of Delaware. N.V. acknowledges support from the National Science Foundation under award number 1507351. W.L. acknowledges support from the Laboratory Directed Research and Development Program of Los Alamos National Laboratory (LANL) under project number 20210087DR. LANL is operated by Triad National Security, LLC, for the National Nuclear Security Administration of the U.S. Department of Energy (Contract No. 89233218CNA000001). X.C. and S.H.W. acknowledge the support from the Beijing Science and Technology Committee (No. Z181100005118003), the National Nature Science Foundation of China (No. 51672023; 11634003; U1930402) and computational support from the Beijing Computational Science Research Center (CSRC), and support from the China Scholarship Council (No. 201904890014).

REFERENCES

(1) Shafarman, W. N.; Klenk, R.; McCandless, B. E. Device and material characterization of Cu(InGa)Se_2 solar cells with increasing band gap. *J. Appl. Phys.* **1996**, *79*, 7324−7328.

(2) Sinton, R.; Cuevas, A.A quasi-steady-state open-circuit voltage method for solar cell characterization. In *Proceedings of the 16th European Photovoltaic Solar Energy Conference*, Glasgow, UK, 2000; pp 1152−1155.

(3) Bowden, S.; Rohatgi, A.Rapid and accurate determination of series resistance and fill factor losses in industrial silicon solar cells. In *Proceedings of the 17th European Photovoltaic Solar Energy Conference*, Munich, Germany, 2001; pp 1802−1805.

(4) Minemoto, T.; Hashimoto, Y.; Shams-Kolahi, W.; Satoh, T.; Negami, T.; Takakura, H.; Hamakawa, Y. Control of conduction band offset in wide-gap Cu(In,Ga)Se_2 solar cells. *Sol. Energy Mater. Sol. Cells* **2003**, *75*, 121−126.

(5) Gokmen, T.; Gunawan, O.; Todorov, T. K.; Mitzi, D. B. Band tailing and efficiency limitation in kesterite solar cells. *Appl. Phys. Lett.* **2013**, *103*, 103506.

(6) Ablekim, T.; Duenow, J. N.; Zheng, X.; Moutinho, H.; Moseley, J.; Perkins, C. L.; Johnston, S. W.; O'Keefe, P.; Colegrove, E.; Albin, D. S.; Reese, M. O.; Metzger, W. K. Thin-Film Solar Cells with 19% Efficiency by Thermal Evaporation of CdSe and CdTe. *ACS Energy Letters* **2020**, *5*, 892−896.

(7) Ye, J.; Soeda, S.; Nakamura, Y.; Nittono, O. Crystal Structures and Phase Transformation in IIn_2Se_3 Compound Semiconductor. *Jpn. J. Appl. Phys.* **1998**, *37*, 4264−4271.

(8) Amory, C.; Bernède, J. C.; Marsillac, S. Study of a growth instability of γ-In_2Se_3. *J. Appl. Phys.* **2003**, *94*, 6945−6948.

(9) Lyu, D. Y.; Lin, T. Y.; Chang, T. W.; Lan, S. M.; Yang, T. N.; Chiang, C. C.; Chen, C. L.; Chiang, H. P. Structural and optical characterization of single-phase γ-In_2Se_3 films with room-temperature photoluminescence. *J. Alloys Compd.* **2010**, *499*, 104−107.

(10) Zheng, Z.; Yao, J.; Xiao, J.; Yang, G. Synergistic Effect of Hybrid Multilayer In_2Se_3 and Nanodiamonds for Highly Sensitive Photodetectors. *ACS Appl. Mater. Interfaces* **2016**, *8*, 20200−20211.

(11) De Groot, C. H.; Moodera, J. S. Growth and characterization of a novel In_2Se_3 structure. *J. Appl. Phys.* **2001**, *89*, 4336−4340.

(12) Julien, C.; Chevy, A.; Siapkas, D. Optical properties of In_2Se_3 phases. *Phys. Status Solidi A* **1990**, *118*, 553−559.

(13) Chaiken, A.; Nauka, K.; Gibson, G. A.; Lee, H.; Yang, C. C.; Wu, J.; Ager, J. W.; Yu, K. M.; Walukiewicz, W. Structural and Electronic Properties of Amorphous and Polycrystalline In_2Se_3 Films. *J. Appl. Phys.* **2003**, *94*, 2390−2397.

(14) Ohtake, Y.; Okamoto, T.; Yamada, A.; Konagai, M.; Saito, K. Improved performance of Cu(InGa)Se_2 thin-film solar cells using evaporated Cd-free buffer layers. *Sol. Energy Mater. Sol.* **1997**, *49*, 269−275.

(15) Nakayama, T.; Fujita, K. Chirality and electronic/optical properties of screw-vacancy In_2Se_3. *AIP Conf. Proc.* **2005**, *772*, 173−174.

(16) Contreras, M. A.; Gabor, A. M.; Tennant, A. L.; Asher, S.; Tuttle, J.; Noufi, R. Accelerated publication 16.4% total area conversion efficiency thin film polycrystalline MgF2/ZnO/CdS/Cu(In,Ga)Se_2/Mo solar cell. *Prog. Photovoltaics* **1994**, *2*, 287−292.

(17) Gordillo, G.; Calderon, C. CIS thin film solar cells with evaporated InSe buffer layers. *Energy Mater. Sol.* **2003**, *77*, 163−173.

(18) Emziane, M.; Le Ny, R. Synthesis and properties of In2(Se1-xTex)3 thin films: A new semiconductor compound. *Appl. Phys. A: Mater. Sci. Process.* **2001**, *72*, 73−79.

(19) Pankove, J. I.*Optical Processes in Semiconductors*; Dover: New York, 1975.

(20) Hohenberg, P.; Kohn, W. Inhomogeneous electron gas. *Phys. Rev.* **1964**, *136*, B864−B871.

(21) Kohn, W.; Sham, L. J. Self-Consistent Equations Including Exchange and Correlation Effects. *Phys. Rev.* **1965**, *140*, A1133−A1138.

(22) Kresse, G.; Hafner, J. Ab initio molecular dynamics for liquid metals. *Phys. Rev. B* **1993**, *47*, 558−561.

(23) Kresse, G.; Hafner, J. Ab initio molecular dynamics for open-shell transition metals. *Phys. Rev. B* **1993**, *48*, 13115−13118.

(24) Blöchl, P. E. Projector augmented-wave method. *Phys. Rev. B* **1994**, *50*, 17953−17979.

(25) Kresse, G.; Joubert, D. From ultrasoft pseudopotentials to the projector augmented-wave method. *Phys. Rev. B* **1999**, *59*, 1758−1775.
(26) Perdew, J. P.; Ruzsinszky, A.; Csonka, G. I.; Vydrov, O. A.; Scuseria, G. E.; Constantin, L. A.; Zhou, X.; Burke, K. Restoring the Density-Gradient Expansion for Exchange in Solids and Surfaces. *Phys. Rev. Lett.* **2008**, *100*, 136406.
(27) Heyd, J.; Scuseria, G. E.; Ernzerhof, M. Hybrid functionals based on a screened Coulomb potential. *J. Chem. Phys.* **2003**, *118*, 8207−8215.
(28) Heyd, J.; Scuseria, G. E.; Ernzerhof, M. Erratum: Hybrid functionals based on a screened Coulomb potential [J. Chem. Phys. 118, 8207 (2003)]. *J. Chem. Phys.* **2006**, *124*, 219906.
(29) Adachi, S.*Properties of Group-IV, III-V and II-VI Semiconductors*; John Wiley & Sons: New York, 2005.
(30) Toll, J. S. Causality and the dispersion relation: Logical foundations. *Phys. Rev.* **1956**, *104*, 1760−1770.
(31) Zunger, A.; Wei, S.-H.; Ferreira, L. G.; Bernard, J. E. Special quasirandom structures. *Phys. Rev. Lett.* **1990**, *65*, 353−356.
(32) Wei, S.-H.; Ferreira, L. G.; Bernard, J. E.; Zunger, A. Electronic properties of random alloys: Special quasirandom structures. *Phys. Rev. B* **1990**, *42*, 9622−9649.
(33) Van de Walle, A.; Tiwary, P.; De Jong, M.; Olmsted, D. L.; Asta, M.; Dick, A.; Shin, D.; Wang, Y.; Chen, L. Q.; Liu, Z. K. Efficient stochastic generation of special quasirandom structures. *CALPHAD* **2013**, *42*, 13−18.
(34) Pfitzner, A.; Lutz, H. Redetermination of the Crystal Structure of γ-In_2Se_3 by Twin Crystal X-Ray Method. *J. Solid State Chem.* **1996**, *124*, 305−308.
(35) Peng, H.; Zhang, X.; Twesten, R.; Cui, Y. Vacancy ordering and lithium insertion in III2VI3 nanowires. *Nano Research* **2009**, *2*, 327−335.
(36) Han, G.; Chen, Z. G.; Drennan, J.; Zou, J. Indium selenides: Structural characteristics, synthesis and their thermoelectric performances. *Small* **2014**, *10*, 2747−2765.
(37) Cui, J.; Peng, H.; Song, Z.; Du, Z.; Chao, Y.; Chen, G. Significantly Enhanced Thermoelectric Performance of γ-In_2Se_3 through Lithiation via Chemical Diffusion. *Chem. Mater.* **2017**, *29*, 7467−7474.
(38) Togo, A.; Tanaka, I. First principles phonon calculations in materials science. *Scr. Mater.* **2015**, *108*, 1−5.
(39) Sreekumar, R.; Jayakrishnan, R.; Sudha Kartha, C.; Vijayakumar, K. P.; Khan, S. A.; Avasthi, D. K. Enhancement of band gap and photoconductivity in gamma indium selenide due to swift heavy ion irradiation. *J. Appl. Phys.* **2008**, *103*, 023709.
(40) Emziane, M; Marsillac, S; Ouerfelli, J; Bernede, J.; Le Ny, R γ-In_2Se_3 thin films obtained by annealing sequentially evaporated In and Se layers in flowing argon. *Vacuum* **1997**, *48*, 871−878.
(41) Groot, C. H.; Moodera, J. S. Growth and characterization of a novel In_2Se_3 structure. *J. Appl. Phys.* **2001**, *89*, 4336−4340.
(42) Wei, S.-H.; Zunger, A. Band offsets at the CdS/$CuInSe_2$ heterojunction. *Appl. Phys. Lett.* **1993**, *63*, 2549−2551.
(43) Grüneis, A.; Kresse, G.; Hinuma, Y.; Oba, F. Ionization Potentials of Solids: The Importance of Vertex Corrections. *Phys. Rev. Lett.* **2014**, *112*, 096401.
(44) Li, W.; Sabino, F. P.; Crasto de Lima, F.; Wang, T.; Miwa, R. H.; Janotti, A. Large disparity between optical and fundamental band gaps in layered In_2Se_3. *Phys. Rev. B* **2018**, *98*, 165134.
(45) Yang, J.; Wei, S.-H. First-principles study of the band gap tuning and doping control in CdSe x Te1-x alloy for high efficiency solar cell. *Chin. Phys. B* **2019**, *28*, 086106.
(46) Wei, S.-H.; Zhang, S. B.; Zunger, A. First-principles calculation of band offsets, optical bowings, and defects in CdS, CdSe, CdTe, and their alloys. *J. Appl. Phys.* **2000**, *87*, 1304−1311.
(47) Vegard, L. Die Konstitution der Mischkristalle und die Raumfüllung der Atome. *Zeitschrift für Physik* **1921**, *5*, 17−26.
(48) Ferreira, L. G.; Wei, S.-H.; Zunger, A. First-principles calculation of alloy phase diagrams: The renormalized-interaction approach. *Phys. Rev. B* **1989**, *40*, 3197−3231.
(49) Bernard, J. E.; Zunger, A. Electronic structure of ZnS, ZnSe, ZnTe, and their pseudobinary alloys. *Phys. Rev. B* **1987**, *36*, 3199−3228.
(50) Wei, S.-H.; Zunger, A. Band offsets and optical bowings of chalcopyrites and Zn-based II-VI alloys. *J. Appl. Phys.* **1995**, *78*, 3846−3856.
(51) Tit, N.; Obaidat, I. M.; Reshak, A. H.; Alawadhi, H. Existence or absence of bandgap bowing in II-VI ternary alloys: Comparison between common-anion and common-cation cases. *J. Phys. Conf. Ser.* **2010**, *209*, 012024.
(52) Rühle, S. Tabulated values of the Shockley-Queisser limit for single junction solar cells. *Sol. Energy* **2016**, *130*, 139−147.

https://doi.org/10.1021/acs.jpclett.2c02975
J. Phys. Chem. Lett. 2022, 13, 12026−12031